# Dual stimuli-responsive oligo(ethylene glycol)-based microgels: insight into the role of internal structure in volume phase transitions and loading of magnetic nanoparticles to design stable thermoresponsive hybrid microgels

Mohamed Boularas, Elise Deniau-Lejeune, Valérie Alard, Jean-François Tranchant, Laurent Billon, Maud Save

# Dual stimuli-responsive oligo(ethylene glycol)-based microgels: insight into the role of internal structure in volume phase transitions and loading of magnetic nanoparticles to design stable thermoresponsive hybrid microgels.

Mohamed Boularas,[a,b] Elise Deniau-Lejeune, [a] Valérie Alard, [b] Jean-François Tranchant, [b] Laurent Billon[a*] and Maud Save [a*]

[a] Université de Pau & Pays Adour, CNRS, UMR 5254, IPREM, Equipe de Physique et Chimie des Polymères, 2 avenue du Président Angot, Pau, F-64053, France

[b] LVMH Recherche Parfums et Cosmétiques, 185 Av. de Verdun, St Jean de Braye, F-45804, France

*E-mail maud.save@univ-pau.fr, laurent.billon@univ-pau.fr

Electronic Supplementary Information (ESI) available.

## ABSTRACT

Multi-responsive biocompatible microgels with long term stability were synthesized by precipitation copolymerization of oligo(ethylene glycol) methyl ether methacrylate (OEGMA), di(ethylene glycol) methyl ether methacrylate ($MEO_2MA$), methacrylic acid (MAA) and crosslinker in aqueous dispersed media. Different crosslinkers, *i.e.* ethylene glycol dimethacrylate (EGDMA), oligo(ethylene glycol) diacrylate (OEGDA) or *N*,*N*-methylenebisacrylamide (MBA) were used for the synthesis of the microgels. The present work investigates for the first time how the inner structure of the biocompatible P($MEO_2MA$-*co*-OEGMA-*co*-MAA) microgels impacts their swelling-to-collapse transition in response to both temperature and pH. The EGDMA-crosslinked microgels obviously differ from the OEGDA- and MBA-crosslinked microgels. The OEGDA-crosslinked P($MEO_2MA$-*co*-OEGMA-*co*-MAA) microgels are ideal candidates to prepare robust thermoresponsive hybrid magnetic microgels by a straightforward method involving simple loading of pre-formed magnetic nanoparticles (NP) in the absence of NP release. The crosslinker distribution is at the origin of differences in the distribution of iron oxide nanoparticles. The homogeneous distribution of both MAA units and OEGDA crosslinker in the P($MEO_2MA$-*co*-OEGMA-*co*-MAA) microgels ensured a sharp VPTT of microgels over a wide range of pH (from pH 4 to 9) and the retention of the thermoresponsiveness of the corresponding hybrid microgels for the different contents of magnetic nanoparticles (from 7 to 33 wt-% of $\gamma$-$Fe_2O_3$ versus polymer). Turbidimetry

measurements highlighted the unique stability of the hybrid microgels over several hours even for the highest content of iron oxide nanoparticles.

## Introduction

Dual stimuli-responsive microgels are micron or submicron crosslinked colloids that are simultaneously sensitive to two external stimuli such as temperature, pH or ionic strength. [1-5] The temperature-induced conformational change of the polymer chains[6-8] involved in the network confers to the microgels the property to undergo a thermoresponsive swelling-to-collapse transition at the volume phase transition temperature (VPTT). The incorporation of a functional co-monomer (carboxylic acid, amine) by random copolymerization provides additional pH- or ionic strength sensitivity to the "smart" microgels.[1, 9] Stimuli-responsive microgels are attractive materials for various fields of application such as drug delivery vectors,[10-14] sensors design,[15, 16] or stabilizers of pickering emulsions.[17, 18] A fine tuning of swelling and shrinkage is of great importance for controlling the final properties of these materials. In addition, the incorporation of inorganic nanoparticles within stimuli-responsive microgels is an interesting strategy to combine their inherent functionalities with those of the microgels.[19, 20] For instance, metallic, magnetic or semi-conductor nanoparticles are able to induce respectively catalytic, magnetic and tunable optical properties to the microgels dispersed in water.[21-23]

Up to now, a large number of studies devoted to the design of multi-responsive microgels dealt with poly(*N*-isopropylacrylamide), a polymer exhibiting a VPTT at ~32 °C. It emerged from these studies that the swelling properties of the PNiPAM-based microgels were strongly dependent on their inner structure, given by the distribution of both the pH-responsive co-monomer and the crosslinker within the microgel.[24, 25] For instance, microgels with well-separated carboxylic acid group showed intense pH-induced swelling while limited swelling was reported with closed-pack distribution of carboxylic acid groups into the microgels.[26, 27] Densely core crosslinked microgels with dangling polymer chains or homogeneously crosslinked PNIPAM-based microgels showed different thermoresponsive phase transition.[28-30] However, the toxicity of the acrylamide monomers and the low level of biocompatibility of PNiPAM might limit the use of such microgels for cosmetic or biomedical concerns.[31] Poly(*N*-vinylcaprolactam) (PVCL) microgels, exhibiting a VPTT of 32 – 36 °C, were reported as biocompatible colloids to offer an alternative to PNiPAM for biomedical applications.[32, 33] Notice that the introduction of carboxylic acid-based co-monomer into PVCL microgels requires specific attention due to the fact that VCL monomer is prone to hydrolysis under acidic

conditions.[34] In parallel, copolymers of oligo(ethylene glycol) methacrylates (OEGMA) with different numbers of ethylene glycol units have received an increasing interest since they gather biocompatibility [35-38] with tunable and sharp volume phase transition. [39-41] Few studies have reported the synthesis of OEGMA-based thermoresponsive microgels, either to produce colloidal crystals by self-assembly of the monodisperse microgels, or to design core-shell microgels for drug uptake and release applications or to investigate the adsorption of thermoresponsive microgels onto solid substrates.[42-46]

The present study will describe the synthesis of a series of multiresponsive carboxylic acid functionalized P($MEO_2MA$-*co*-OEGMA-*co*-MAA) microgels in order to investigate the relationship between the inner structure of such microgels and their swelling-to-collapse transition in response to both pH and temperature stimuli. These microgels are of interest from the biocompatibility of oligo(ethylene glycol) methacrylate based copolymers[35-38] and of oligo(methacrylic acid) residues (MAA copolymers were approved by Food and Drug Administration for delayed drug release capsules or oral suspensions). Moreover, hybrid thermoresponsive magnetic microgels will be prepared by loading an aqueous dispersion of pre-formed maghemite nanoparticles (NPs) into the swollen carboxylic acid-functionalized oligo(ethylene glycol)-based microgels. The method of post-loading a dispersion of NPs[47] has been scarcely investigated in comparison with the in-situ synthesis of NPs by salt reduction from the microsphere template.[21, 48] This was mainly due to difficulties in achieving high concentration of NPs while limiting their aggregation and release.[47] However, this method deserved our attention as it represents an efficient way to prepare hybrid magnetic microgels from two distinct aqueous dispersion of colloids and does not require the implementation of chemical reaction involving a reductive agent inside the microgels. This strategy should ease material handling for industrial sector.The present work reports that P($MEO_2MA$-*co*-OEGMA-*co*-MAA) microgels offer the unique opportunity to quantitatively load high content of pre-formed magnetic NPs (up to 33 wt-% vs. microgel). It will be shown that the structure of the present microgels is a key to overcome for the first time the issue of nanoparticle desorption previously encountered when loading pre-formed magnetic nanoparticles into thermoresponsive microgels. Finally, the stability of both the P($MEO_2MA$-*co*-OEGMA-*co*-MAA) microgels and the corresponding hybrid microgels will be thoroughly investigated by turbidimetry measurements. .

## Experimental Part

**Materials.** Di(ethylene glycol) methyl ether methacrylate ($MEO_2MA$ 95%, Aldrich), oligo(ethylene glycol) methyl ether methacrylate (OEGMA, monomethyl terminated with 8 EG repeat units, number average weight Mn = 475 $g.mol^{-1}$, Aldrich), methacrylic acid (MAA, Aldrich), poly(ethylene glycol)diacrylate (OEGDA, number average weight Mn = 250 $g.mol^{-1}$, Aldrich), *N*,*N*-methylenebisacrylamide (MBA, Aldrich), (ethylene glycol)dimethacrylate (EGDMA, Aldrich) and potassium persulfate (KPS 99%, ABCR) were used as received for the synthesis of P(NIPAM-*co*-MAA) and P($MEO_2MA$-*co*-OEGMA-*co*-MAA) microgels. Hydrochloric acid (HCl, 36%w/w, ABCR) and potassium hydroxide (KOH, Aldrich) were used to monitor pH of solution. All water used in the synthesis and characterization was purified using a Millipore Milli-Q system. Iron (II) chloride tetrahydrate ($FeCl_2.4H_2O$, Aldrich), iron (III) chloride hexahydrate ($FeCl_3.6H_2O$, $6H_2O$, Aldrich), ferric nitrate ($Fe(NO_3)_3$, Aldrich), ammonium hydroxide ($NH_4OH$, 28-30 %w/w, Aldrich), nitric acid ($HNO_3$, Aldrich) and hydrochloric acid (HCl, 36 wt-%, ABCR) were used for the synthesis of maghemite nanoparticles without further purification (see Electronic Supporting Information).

**Synthesis of P($MEO_2MA$-*co*-OEGMA-*co*-MAA) microgels.** P($MEO_2MA$-*co*-OEGMA-*co*-MAA) microgels were synthesized by precipitation copolymerization in aqueous dispersed media. The microgels are prepared by precipitation copolymerization of di(ethylene glycol) methyl ether methacrylate ($MEO_2MA$), oligo(ethylene glycol) methyl ether methacrylate (OEGMA) and methacrylic acid (MAA) in the presence of crosslinker (EGDMA, OEGDA or MBA) and potassium persulfate (KPS) as initiator. All reactants are first soluble in water and the polymer chains precipitate during the copolymerization to form crosslinked colloidal particles stabilized by the anionic charges of the initiator. The initial solid content was set at 2.3 wt-% (+/- 0.2) for all synthesis performed. Crosslinker and initiator KPS were kept constant at 1.92 mol-% and 0.86 mol-% versus the total number of moles of vinylic molecules. Briefly, the $MEO_2MA$, OEGMA (0.272 g, 0.573 mmol) and crosslinker (e.g. OEGDA: 0.029 g, 0.117 mmol) were dissolved in 57.5 mL of water. The reaction mixture was first introduced in a 250 mL 3-neck round-bottom flask equipped with a mechanical stirrer (set at 30 rpm) and purged with nitrogen for 45 min at room temperature to remove oxygen. A solution of MAA (0.026 g, 0.305 mmol dissolved in 2 mL of water) was then introduced into the reaction media. The mixture was heated up to 70 °C for 30 min and KPS solution (14.3 mg of KPS dissolved in 2.5 mL of degassed water) was introduced in order to initiate the polymerization. The reaction mixture became turbid after few minutes and was maintained at 70 °C for 6 h to complete the reaction. Instantaneous conversions of $MEO_2MA$, OEGMA, MAA and crosslinkers were

studied by NMR spectroscopy. Precipitation polymerization of the P($MEO_2MA$-*co*-OEGMA-*co*-MAA) microgels was performed in water and trioxane was used as internal standard. Samples were withdrawn at different time interval diluted in deuterium oxide ($D_2O$) to achieve a ratio 9:1 of $H_2O$:$D_2O$.

Monomer conversions were determined by equation (1) using the integration of monomer vinyl protons and alkyl proton of internal standard (see Figure SI-1 in ESI):

$$x = 1 - \frac{[M]_t}{[M]_0} = 1 - \frac{[M]_t/[\text{Trioxane}]_t}{[M]_0/[\text{Trioxane}]_0} = 1 - \frac{I_{M,t}/I_{trioxane,t}}{I_{M,0}/I_{trioxane,0}} \quad (1)$$

$I_M$ and $I_{Trioxane}$ are the proton integral values of monomer M and internal standard at initial time $t_0$ and sampling time t.

$^1$H NMR ($H_2O$:$D_2O$ 9:1, 400 MHz): **$MEO_2MA$:** δ (ppm): 1.85 (s, 3H, (C=C-**$CH_3$**)), 3.3 (s, 3H, O-**$CH_3$**), 3.54 (d, 2H, O-$CH_2$-**$CH_2$**-O-$CH_3$), 3.64 (d, 2H, O-**$CH_2$**-$CH_2$-O-$CH_3$), 3.74 (d, 2H, C=C-(OC)-O-$CH_2$-**$CH_2$**-O-), 4.26 (d, 2H, C=C-(OC)-O-**$CH_2$**-$CH_2$-O-), 5.65 (dd, 1H, (**$H_{trans}$**-HC=C($CH_3$)-C(=O)O-)), 6.1 (dd, 1H, (**$H_{cis}$**-HC=CH($CH_3$)-C(=O)O-)). **OEGMA (Mn 475):** δ (ppm): 1.85 (s, 3H, (C=C-**$CH_3$**)), 3.3 (s, 3H, O-**$CH_3$**), 3.54 (d, 2H, O-$CH_2$-**$CH_2$**-O-$CH_3$), 3.64 (d, 26-30H, O-**$CH_2$**-$CH_2$-O-$CH_3$), 3.74 (d, 2H, C=C-(OC)-O-$CH_2$-**$CH_2$**-O-), 4.26 (d, 2H, C=C-(OC)-O-**$CH_2$**-$CH_2$-O-), 5.65 (dd, 1H, (**$H_{trans}$**-HC=C($CH_3$)-C(=O)O-)), 6.1 (dd, 1H, (**$H_{cis}$**-HC=C($CH_3$)-C(=O)O-)), **MAA:** δ (ppm): 1.81 (s, 3H, C=C-(**$CH_3$**)). 5.55 (dd, 1H, **$H_{trans}$**-HC=C($CH_3$)-C(=O)OH)). 5.93 dd, 1H, **$H_{cis}$**-HC=C($CH_3$)-C(=O)OH)), **OEGDA (Mn 250):** δ (ppm): 3.64 (d, 16-12H, O-**$CH_2$**-$CH_2$-O-), 3.74 (d, 4H, C=C-(OC)-O-$CH_2$-**$CH_2$**-O-), 4.26 (d, 4H, C=C-(OC)-O-**$CH_2$**-$CH_2$-O-), 5.92 (dd, 1H, (**$H_{trans}$**-HC=CH-C(=O)O-)), 6.1 (dd, 1H, ($H_2$C=C**H**-C(=O)O-)), 6.36 (dd, 1H, (**$H_{cis}$**-HC=CH-C(=O)O-)), **EGDMA:** δ (ppm): 2.15 (s, 6H, (C=C-**$CH_3$**)), 4.25 (d, 4H, C=C-(OC)-O-**$CH_2$**-$CH_2$-O-), 5.65 (dd, 2H, (**$H_{trans}$**-HC=C($CH_3$)-C(=O)O-)), 6.03 (dd, 2H, (**$H_{cis}$**-HC=C($CH_3$)-C(=O)O-)), **MBA:** δ (ppm): 4.2 (s, 2H, NH-(**$CH_2$**)-NH). 5.7 (dd, 2H, H(OC-)C=C-**$H_{cis}$**(-H)). 6.15 (dd, 2H, H(OC-)C=C-**$H_{trans}$**(-H) / dd, 2H, $H_2$C=C(-CO)-**H**), **trioxane:** δ(ppm)= 5.1 (s, 3H, (O-**$CH_2$**)).

The microgels were then purified by 5 centrifugation/redispersion cycles (10.000 rpm, 30 min) with milliQ grade water and finally stored at room temperature. The fraction of water-soluble polymer (WSP) was determined by gravimetric analyses of the supernatant collected during centrifugation of the microgel dispersion.

**Synthesis of γ-$Fe_2O_3$-P($MEO_2MA$-*co*-OEGMA-*co*-MAA) hybrid microgels.** The hybrid γ-$Fe_2O_3$-P($MEO_2MA$-co-OEGMA-co-MAA) microgels were prepared by encapsulation of cationic γ-$Fe_2O_3$ nanoparticle into the stimuli-responsive OEGMA-based microgels.[59] Typically, 40 mL of microgel dispersion at 1.45 g.L$^{-1}$ was introduced into a round bottom flask

and the pH was adjusted to 3.0 by addition of nitric acid solution ($HNO_3$ 0.1M). The cationic maghemite nanoparticles dispersed in water were prepared from the Massart method (see details in ESI).[49, 50] The cationic ferrofluid (10 mL at 1.34 $g.L^{-1}$) was added dropwise to the aqueous microgel dispersion under continuous stirring at room temperature and was kept overnight under stirring. The pH of the aqueous solution of microgels was then adjusted to 7.0 by addition of alkaline solution (KOH, 0.5M) in order to destabilize the magnetic nanoparticles into the microgel structure while promoting the stability of the final hybrid microgel by the potassium carboxylate functions. Finally the dispersion was purified by 5 centrifugation/redispersion (5.000 rpm, 10 min).

**Carboxylic acid titration**. Salt-free base-into-acid titrations were performed by coupling conductometric and potentiometric techniques as previously described.[51] Samples were prepared by suspending 50 mg of freeze-dried microgel in 30 mL of pure water and pH of dispersion was adjusted below 3.0 with hydrochloric acid (HCl) 0.1 M solution in order to fully protonate the carboxylic groups. A graphite electrode connected to a CDM230 conductivity meter (Radiometer Analytical, France) and SenTix 81 pH-electrode connected to WTW pH3310 pH-meter (WTW GmbH, Germany) were used in the microgel dispersions under continuous stirring. Then sodium hydroxide (NaOH) solution (1.5 mM) freshly prepared were used. The degree of ionization at 20°C ($\alpha_{20°C}$) and the apparent acid dissociation constant ($pK_a$) were calculated from titration data on the basis of equations 2 and 3.

$$\alpha_{20°C} = \frac{[MA^-Na^+]}{[MA^-Na^+] + [MAA]} = \frac{V_{NaOH,1mM} - V_{eq1}}{V_{eq2} - V_{eq1}} \quad (2)$$

$$pK_a = pH - log\left(\frac{\alpha_{20°C}}{1 - \alpha_{20°C}}\right) \quad (3)$$

**NMR**. Proton nuclear magnetic resonance spectra were recorded using a Brüker 400 MHz spectrometer at 25 °C.

**DLS.** The hydrodynamic diameters ($D_h$) were measured by Dynamic Light Scattering (DLS) with a Vasco-2 Particle Size Analyzer from Cordouan Technologies (Pessac, France) working at an angle of 135° and a wavelength of 658 nm. Autocorrelation functions were recorded using a multi-acquisition mode and apparent diffusion coefficients were determined via the Pade-Laplace inverse algorithm and the second-order cumulant methods of a large number of measurements. Hydrodynamic diameter was calculated from the Stokes-Einstein equation (Eq. (4)) and polydispersity index (PDI) is given by the cumulant analysis method.

$$D_z = \frac{k_B T}{6\pi.\eta.R_h} \quad (4)$$

Where $k_B$ is the Boltzmann constant, $T$ is the absolute temperature, η is the viscosity of the medium, $R_h$ is the hydrodynamic radius, and $D_z$ is the apparent diffusion coefficient.

The final number of particles ($N_p$) was calculated from equation (5). According to reference 52, an average content of 30 % of water content inside the microgel at collapsed was taken into account.

$$N_p = 6.\frac{\left(\frac{\tau_{polymer} - WSP}{\rho_{polymer}}\right) + 0.3\left(\frac{\tau_{polymer} - WSP}{\rho_{H20}}\right)}{\pi.D_h^3} \quad (5)$$

Where $\tau$ is the final solid content of the reaction media, WSP (in $g.L^{-1}$) is the fraction of water soluble polymer in the final dispersion, $\rho_{polymer}$ ($g.m^{-3}$) is the density of the polymer. We assumed the density of collapsed P(OEGMA-*co*-$MEO_2MA$) similar to the one of a linear poly(ethylene glycol) ($\rho_{PEG}$ = 1.2 $g.cm^{-3}$).[53] $D_h$ is the hydrodynamic diameter of aqueous dispersed microgel measured at collapsed state and pH 3 (T = 60°C). For the measurement of the $D_h$ profile versus temperature, the variation of the water viscosity with temperature was considered and samples were left to equilibrate for 15 min before analysis.

**Stability measurements**. Stability of the microgel dispersions were measured with a Turbiscan AGS equipped with near infra-red light source (Formulaction). Microgel dispersions at 2.1 wt-% were introduced into cylindrical cell (Tube height, H= 37 ±1 mm) in which light transmission and backscattering of the microgel dispersions were measured at 30 °C along the tube by using a detection head. Data acquisitions were set every 12 hours and for 30 days at pH 6 for P($MEO_2MA$-*co*-OEGMA-*co*-MAA) microgels while data were recorded every 2 hours for 7 days at pH 7 for the hybrid microgels. See ESI for further details of measurements.

**TEM**. The microgels were characterized by transmission electron microscopy (TEM) in dried state with a Philips CM12 using an accelerating voltage of 120 kV at room temperature. A drop of the aqueous microgels suspension was placed on carbon-coated copper grid (Ted Pella, for TEM), and dried under ambient conditions.

**TGA**. *T*he γ-$Fe_2O_3$ nanoparticles content inside the hybrid microgels were determined by thermogravimetric analyses performed on a TGA Q50, TA Instruments at a heating rate of $10°C.min^{-1}$ under nitrogen.**Results and discussion**

*Synthesis and colloidal features of P($MEO_2MA$-co-OEGMA-co-MAA) microgels.*

The P($MEO_2MA$-*co*-OEGMA-*co*-MAA) microgels were synthesized by aqueous batch precipitation copolymerization of di(ethylene glycol) methyl ether methacrylate ($MEO_2MA$), oligo(ethylene glycol) methyl ether methacrylate (OEGMA) and methacrylic acid (MAA) in the presence of 1.9 wt-% of crosslinker. Different difunctional crosslinkers were used: (ethylene

glycol) dimethacrylate (EGDMA), oligo(ethylene glycol) diacrylate (OEGDA) or *N,N*-methylenebisacrylamide (MBA). The polymerization was carried out at 70 °C and was initiated by the addition of potassium persulfate (KPS) initiator. The experimental conditions are summarized in Table 1.

**Table 1: Synthesis and colloidal features of multiresponsive microgels carried out at 70°C.**[a]

| Exp. | $[MEO_2MA]_0$ | $[OEGMA]_0$ | $[MAA]_0$ | [CL] | CL | WSP [b] | $D_{H,60°C}$ (PDI) [c] | $N_p$ [d] |
|---|---|---|---|---|---|---|---|---|
| | *mmol.L$^{-1}$* | *mmol.L$^{-1}$* | *mmol.L$^{-1}$* | *mmol.L$^{-1}$* | | *wt%* | *nm* | *$\times 10^{16}$ L$^{-1}$* |
| **1** | 85.5 | 9.50 | 5.0 | 1.95 | EGDMA | 80 | 513 (0.060) | 6 |
| **2** | 85.6 | 9.56 | 5.0 | 1.92 | OEGDA | 34 | 470 (0.025) | 25 |
| **3** | 85.7 | 9.56 | 5.0 | 1.96 | MBA | 35 | 450 (0.199) | 29 |

[a] The initial OEGMA:$MEO_2MA$ molar ratio is 10:90, the molar ratio of crosslinkers (CL) and initiator (KPS) molar were set at respectively 1.92 mol-% and 0.86 mol-% over the total monomer content. The initial solid content is 2.3 wt-% (+/-0.2). [b] WSP is the weight fraction of water-soluble polymer (in wt%) versus weight of microgel. [c] $D_{H,60°C}$ is the hydrodynamic diameter of the collapsed microgels measured at at pH 3 and at 60 °C. PDI corresponds to the dispersity provided by DLS (dispersity below 0.1 indicates monodisperse colloids). [d] $N_p$ is the number of particles calculated from equation 5.

The individual conversion of each vinylic group was monitored by $^1$H NMR spectroscopy using trioxane as internal standard (Figure SI-1 in ESI).

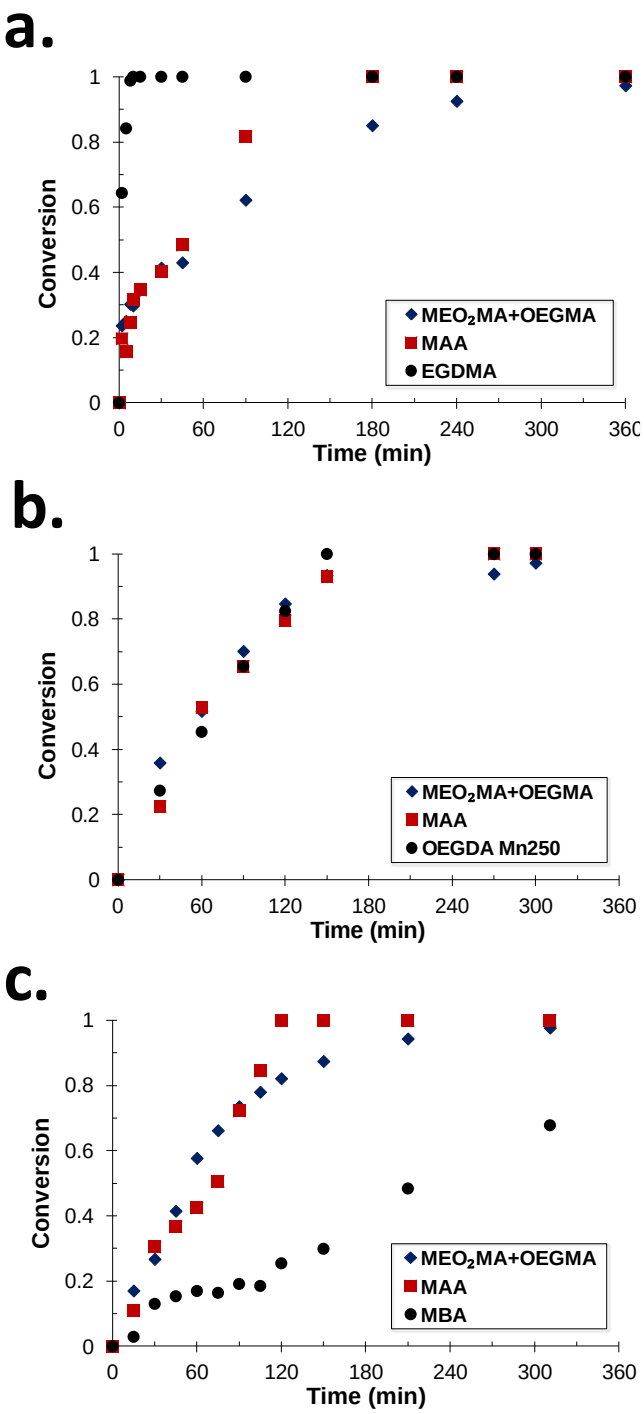


**Figure 1.** Vinylic group conversion conversion versus time of (♦) ($MEO_2MA$ and OEGMA), (■) MAA and (●) crosslinker (a. EGDMA, b. OEGDA ($M_n$ 250), c. MBA).

A fast consumption of EGDMA crosslinker was observed with a complete conversion reached in less than 15 minutes whereas complete conversion of monomers was reached in only 6 hours (Figure 1.a). The high reactivity of EGDMA in precipitation copolymerization can be ascribed to its higher hydrophobicity (value of limited water solubility = 5.4 $mmol.L^{-1}$),[54] favoring its partition towards the hydrophobic nuclei in the early stage of polymerization (Figure 1a). On

the other hand, a perfect overlay of the individual conversion of OEGDA, OEGMA, $MEO_2MA$ and MAA shows a simultaneous consumption of the monofunctional methacrylate monomers and the difunctional acrylate crosslinker during the microgel synthesis (Figure 1b). The *N*,*N*-methylenebisacrylamide (MBA) crosslinker is consumed very slowly in comparison with the methacrylic monomers with only half of the crosslinker polymerized at complete monomer conversion (Figure 1c). For comparison, the synthesis of P(NIPAM-*co*-MAA) microgels showed opposite behavior with a higher reactivity of MBA providing microgels with densely crosslinked core and loosely crosslinked shell.[28, 55-58] The variation of both the crosslinking density ($\Delta\rho_c = (\Delta x_{CL}[CL]_0/\Delta x_M[M]_0$ with $\rho_c$ the number of polymerized (meth)acrylic groups of crosslinker by number of monomer units polymerized into the microgel) and the average molar mass between crosslinks ($M_c = M_{mono}/\Delta\rho_c$) for a given monomer conversion interval ($\Delta x = x_{t2} - x_{t2}$ with $x$ the conversion of vinylic group of crosslinker or monomers in a time interval) are plotted versus the overall monomer conversion (Figure 2 and Figure SI-2 in ESI).

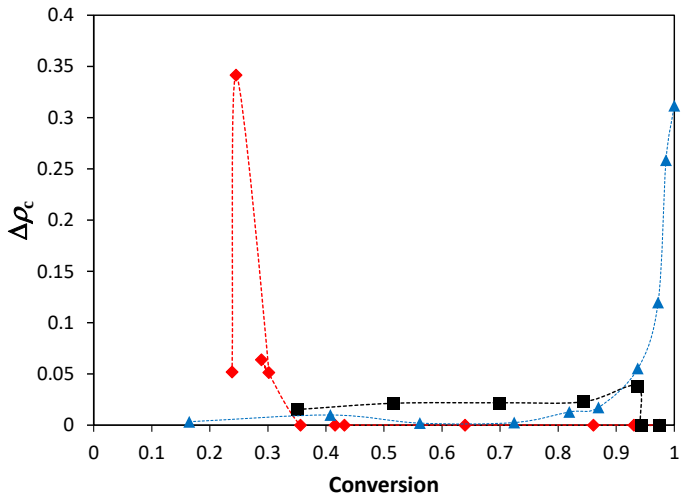


**Figure 2**. Variation of crosslinking density plotted as a function of the overall monomer conversion for different crosslinkers: (♦) EGDMA, (■) OEGDA, (▲) MBA.

One can suggest a heterogeneous distribution of the EGDMA crosslinker within the particle with the production of densely crosslinked core and very loosely crosslinked shell. Indeed, Figure 2 suggests a sharp transition between high values of crosslinking density at the early stage of polymerization towards very low values of $\Delta\rho_c$. Above 35 % of conversion, non-crosslinked chains (infinite $M_c$) are produced as the EGDMA crosslinker is entirely polymerized (Figure SI-2). On the other hand, microgels with homogeneous network are synthesized by using the OEGDA crosslinker with constant values of $\Delta\rho_c$ and $M_c$ (~ 10000 $g.mol^{-1}$) along the polymerization (Figure 2 and Figure SI-2). The continuous slow

polymerization of MBA crosslinker (Figure 1) induces a slightly crosslinked network ($M_c$ ~ 20000 – 120000 g.mol$^{-1}$) in the core of the microgel associated with a sharp increase of the crosslinking density at monomer conversion above 85 % producing a more densely crosslinked shell ($M_c$ < 1000 g.mol$^{-1}$, Figure SI-2).

In summary, the crosslinking distribution can be tuned by a suitable choose of the crosslinker. Three types of P($MEO_2MA$-*co*-OEGMA-*co*-MAA) microgels with different inner structures were synthesized, from homogeneously crosslinked microgels using OEGDA crosslinker to microgels with densely-crosslinked core and loosely-crosslinked shell microstructure using EGDMA crosslinker or microgels exhibiting slightly crosslinked network with densely-crosslinked thin shell using MBA crosslinker (Scheme 1).

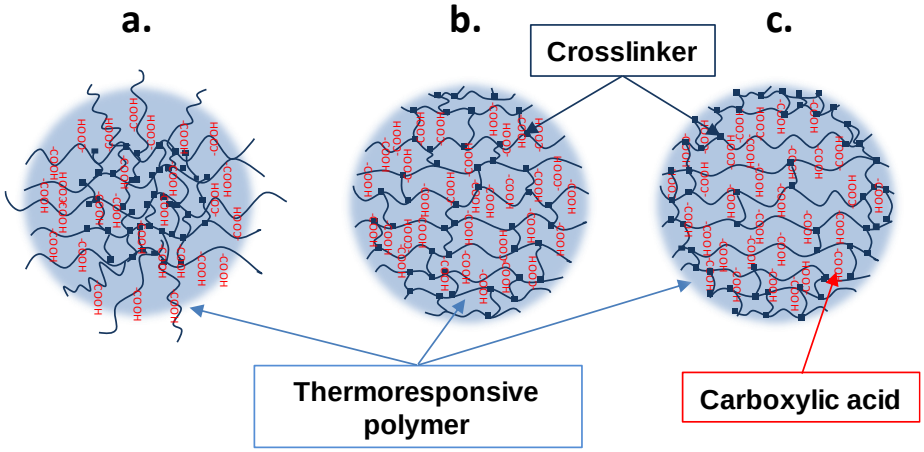


**Scheme 1**. Microstructures of P($MEO_2MA$-*co*-OEGMA-*co*-MAA) microgels synthesized with (a) EGDMA, (b) OEGDA and (c) MBA. Homogeneous MAA distribution and different crosslinking densities: (a) densely crosslinked core and loosely crosslinked shell, (b) homogeneously crosslinked migrogels, (c) crosslinking enrichment in the shell with slightly crosslinked core.

The monitoring of the individual conversions was also efficient to assess the distribution of the methacrylic acid units within the microgels (Figure 1). Whatever the nature of the crosslinker, a quasi-simultaneous consumption of methacrylic acid, OEGMA and $MEO_2MA$ monomers was observed, suggesting a homogenous localization of the pH-sensitive monomer within the microgel. The average ($F_{MAA}$) and instantaneous ($F_{MAA,inst}$) molar fractions of MAA incorporated inside the polymer chains of the microgel were plotted versus the monomer conversion to highlight the quasi-constant value of $F_{MAA}$ along the polymerization (see Figure SI-3 in ESI). In parallel, we investigated the polyelectrolyte properties of the PMAA units inside the microgels. The potentiometric titrations of the microgels in swollen state enabled us to

calculate the degree of ionization $\alpha$ (see equation 7) of the carboxylic acid functions as a function of the pH value (Figure 3).

$$\alpha = \frac{[MA^- Na^+]}{[MA^- Na^+] + [MAA]} \tag{7}$$

The apparent acid dissociation constant ($pK_a$) of the MAA units in the microgel was plotted as a function of the degree of ionization according to equation 8.

$$pK_a = pH - \log(\frac{\alpha}{1-\alpha}) \tag{8}$$

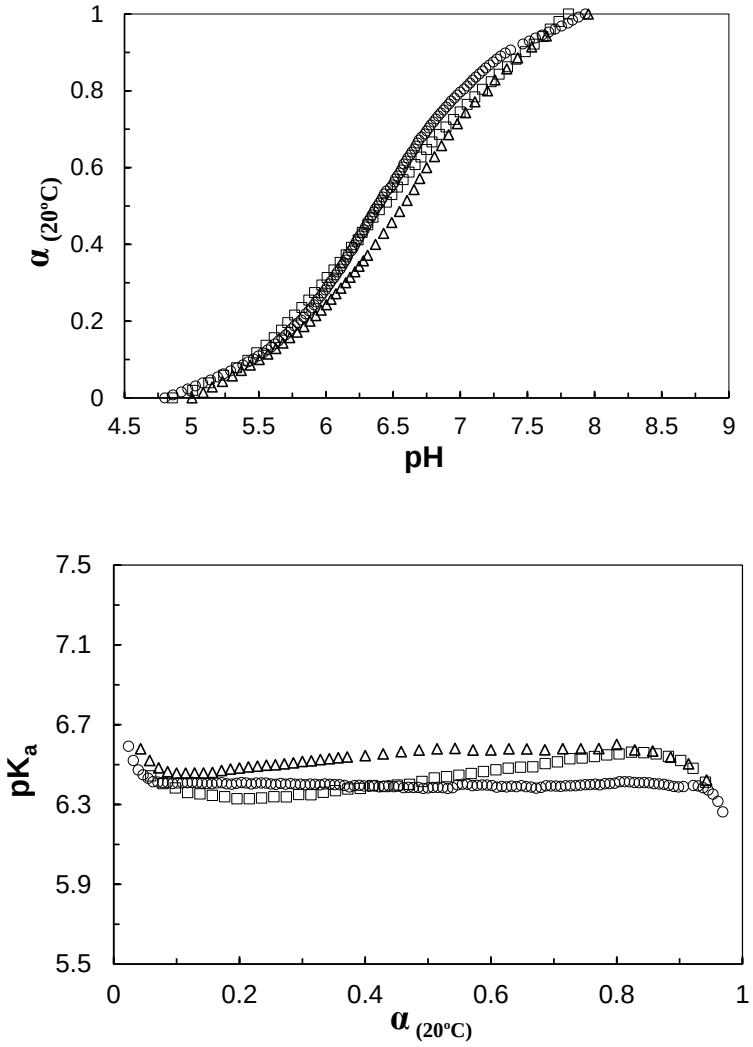


**Figure 3**. (Top) Degree of ionization of MAA versus pH and (bottom) *pK*a values of carboxylic acid group versus $\alpha$ for P($MEO_2MA$-*co*-OEGMA-*co*-MAA) microgels crosslinked with EGDMA (□, expt 2), OEGDA (Δ, expt 4) and MBA (○, expt 6) (T = 25 °C).

The present P($MEO_2$MA-*co*-OEGMA-*co*-MAA) microgels show a monotonous evolution of the degree of ionization versus *pH* with a complete ionization reached at *pH* of 7.9 (Figure 3). It is worth to note that carboxylic acid of the P($MEO_2$MA-*co*-OEGMA-*co*-MAA) microgels exhibit higher values of the apparent acid dissociation constant at half-neutralization point ($pK_{a,\ \alpha=0.5}$ ~ 6.5 +/- 0.1, see Figure 3) in comparison with the linear PMAA homopolymer ($pK_{a,\ \alpha=0.5}$ ~ 4.6 – 5.3).[59] Such increase is characteristic of the burial of the MAA groups inside the constrained polymer network that weaken their acidity even at swollen state. A similar effect was previously observed by Hoare *et al*.[25] for P(NiPAM-*co*-MAA) microgels showing a $pK_{a,\ \alpha=0.5}$ value of 6.3-6.5. The profiles of p$K_a$ versus the degree of ionization are the most relevant data to discriminate the distribution of the carboxylic acid groups within the microgels (Figure 3). For the P($MEO_2$MA-*co*-OEGMA-*co*-MAA) microgels, the value of $pK_a$ remains constant over the range of ionization degree ($\Delta pK_a$ < 0.2), hence supporting the homogeneous distribution of well-isolated carboxylic acid units from the outer to the inner part of the P($MEO_2$MA-*co*-OEGMA-*co*-MAA) microgel. Indeed, the plateau is consistent with the absence of "polyelectrolyte effect", such effect corresponding to an increase of the charges along a polyelectrolyte backbone increasing the excess free energy required to ionize the adjacent groups.[26, 60] For comparison, the P(NIPAM-*co*-MAA) microgels exhibiting a heterogeneous MAA distribution showed an intense deviation of the apparent $pK_a$ ($\Delta pK_a$ ~ 1.7 for $\Delta\alpha$ = 1) in relationship with "blocky" PMAA sequences.[26] Even for P(NIPAM-*co*-AA) microgels exhibiting a better distribution of carboxylic acid units or for P(NIPAM-*co*-MAA) microgels synthesized by continuous feeding of MAA with controlled rate, an increase of $pK_a$ value of 1.0 unit was still observed.[26, 61] The quasi-constant value of $pK_a$ ($\Delta pK_a$ < 0.2) in the P($MEO_2$MA-*co*-OEGMA-*co*-MAA) microgels of the present work (Figure 3) corroborates the homogeneous distribution of MAA units in the polymeric network suggested by the monitoring of the individual conversions (Figure 1 and Figure SI-3). An accurate comparison of the *pK*a versus the degree of ionization (Figure 3) reveals the network dependence of the MAA ionization. Indeed, only the EGDMA-crosslinked microgels shows a slight increase of $pK_a$ of 0.2 units which might translate the more difficult ionization of MAA inside the densely crosslinked core.

The colloidal features of the final microgels, *i.e*. number of particles ($N_p$) and particle size distribution (PDI) are reported in Table 1. Attention was paid to evaluate the yield of microgel formation by measuring the weight fraction of final non-crosslinked polymer, also named water-soluble polymer (WSP). As summarized in Table 1, the chemical nature of the

crosslinker influences concomitantly the fraction of water soluble polymer and the final number of particles. The OEGDA- and MBA-crosslinked P($MEO_2MA$-*co*-OEGMA) microgels display a lower fraction of water-soluble polymer (35 wt %) and a higher number of particles ($N_p \sim 25 - 28 \times 10^{16}$ particles.$L^{-1}$) than the EGDMA crosslinked P($MEO_2MA$-*co*-OEGMA) microgels (80 wt% of WSP, $N_p \sim 6 \times 10^{16}$ particles.$L^{-1}$). As depicted in Figure 1.a, the EGDMA crosslinker being entirely polymerized for an overall monomer conversion below 35 %, the further initiated polymer chains are non-crosslinked chains which are water soluble at 20°C. On the other hand, the monomer polymerization and crosslinker consumption occur concomitantly all along the polymerization for OEGDA and MBA crosslinkers (Figure 1.b-c) producing a lower fraction of WSP (Exp 2 and 3, Table 1). Concerning the number of particles, the strong hydrophobicity of the EGDMA crosslinker together with its fast incorporation might have weakened the stability of the nuclei. A coagulation during the nucleation period decreases the number of particles of the dispersion (Expt 1 in Table 1). Conversely, the nuclei formed by the growing oligo-radicals crosslinked with the more hydrophilic OEGDA and MBA crosslinkers slowly polymerized are more stable. A higher number of final microgel particles was achieved in relationship with a higher number of nuclei (Expt 2 and 3 in Table 1). It can be noticed that the dispersions of P($MEO_2MA$-*co*-OEGMA-*co*-MAA) microgels exhibit a narrow particle size distribution (PDI < 0.1) which is the sign of a short nucleation period and the absence of secondary nucleation.

In summary of this first part, we highlighted that EGDMA crosslinker noticeably influenced the nucleation period to produce dispersions with lower number of microgel particles in comparison with OEGDA- and MBA-crosslinked P($MEO_2MA$-*co*-OEGMA-*co*-MAA) microgels. It was concluded from titration and kinetic data to a homogeneous distribution of well-isolated MAA units. On the basis of the discrepancy in the reactivity of the three crosslinkers, different inner structures of the colloidal networks were suggested as displayed in scheme 1.

*Swelling-to-collapse transition of multi-responsive P($MEO_2MA$-co-OEGMA-co-MAA) microgels.*

This part will be devoted to the investigation of the volume phase transition of the different microgels in response to both temperature and *pH*. The thermoresponsive behavior of the OEGDA-crosslinked P($MEO_2MA$-*co*-OEGMA-*co*-MAA) microgels (Exp. 2 in Table 1) was investigated by dynamic light scattering to plot the evolution of the hydrodynamic diameter

($D_h$) of microgels as a function of temperature at different pH values (Figure 4). In order to scan a degree of ionization from 0 (fully protonated MAA units) to 1 (fully ionized MAA units), the pH of the aqueous dispersion was tuned from 3 to 9, by addition of either hydrochloric acid or potassium hydroxide from the initial dispersion recovered at pH 6.0 after polymerization.

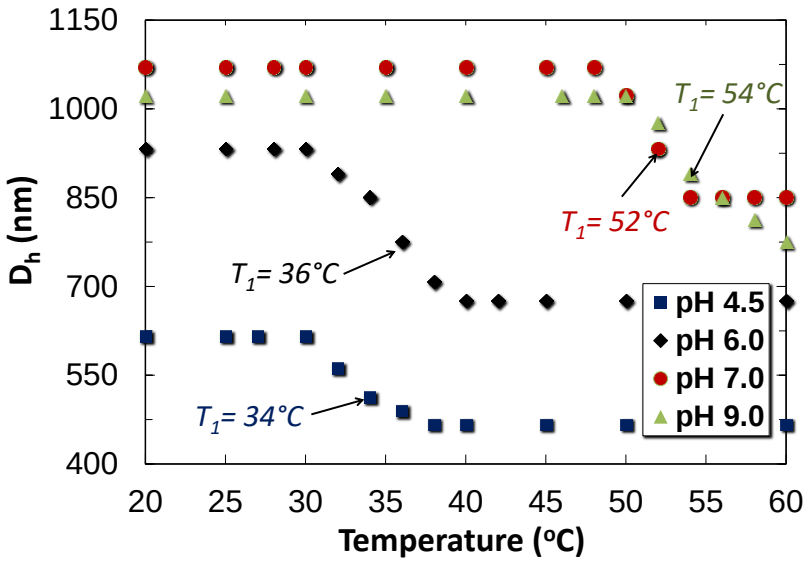


**Figure 4**. Hydrodynamic diameter $D_h$ (nm) of OEGDA-crosslinked P($MEO_2MA$-*co*-OEGMA-*co*-MAA) microgels versus temperature for different pH values.

The profile of the hydrodynamic diameter ($D_h$) versus temperature confirms the thermoresponsive behavior of the P($MEO_2MA$-*co*-OEGMA-*co*-MAA) microgels with their ability to collapse with increasing temperature (Figure 4). The biocompatible OEGDA-crosslinked microgels proved to be concomitantly pH-responsive as the volume phase transition temperature (VPTT) is shifted to higher values by rising the pH of solution ($VPTT_{pH\ 4.5}$ = 34 °C and $VPTT_{pH\ 7}$ = 52 °C $VPTT_{pH\ 9}$ = 54 °C, Figure 4). Such increase of VPTT with pH is assigned to an increase of the degree of ionization of methacrylic acid from $\alpha$ = 0 at pH 4.5 to $\alpha$ = 1 at pH 9, which counterbalances the polymer collapse. It is worth to note that even if the VPTT is shifted to higher temperature, the transition profile of the homogeneously OEGDA-crosslinked microgels remained sharp at any pH ($\Delta T$= 6 - 8 °C, Figure 4). The fast response of the present OEGDA-crosslinked P($MEO_2MA$-*co*-OEGMA-*co*-MAA) microgels with temperature at different pH values highlights the homogeneous environment of the ethylene glycol side-chains, the latter exhibiting a rapid conformational change near the VPTT. It can be noticed that this trend was not observed for PNIPAM-based or PVCL-based multiresponsive microgels. For these later microgels, the ionization of COOH groups strongly influenced the

conformational change of the polymer, which resulted in a broadening of the phase transition temperature.[10, 25, 62] In the case of EGDMA-crosslinked P(MEO$_2$MA-*co*-OEGMA-*co*-MAA) microgels, the broadening of the temperature-induced transition ($\Delta T_{pH\ 4.5}$ = 10 °C, $\Delta T_{pH\ 6.0}$ = 20 °C, Figure SI-4) reveals the impact of the heterogeneous network on the conformation change.

The most relevant behavior of the biocompatible P(MEO$_2$MA-*co*-OEGMA-*co*-MAA) microgels is their unique dual pH and temperature responsiveness. Indeed, among the sharp temperature-induced swelling-to-collapse volume phase transition observed at different pH, the P(MEO$_2$MA-*co*-OEGMA-*co*-MAA) microgels also proved to be highly pH-dependent with an obvious increase of the hydrodynamic diameter by increasing pH (Figure 5). Raising the pH value from 3 to 9 induces a swelling of the P(MEO$_2$MA-*co*-OEGMA-*co*-MAA) microgels with a transition observed between pH 5.5 to pH 6.0. It can be emphasized that such pH-induced transition is present at both swollen state (T = 20°C) and collapsed state (T = 60 °C) while preserving with the ability to undergo a thermoresponsive swelling-to-collapse transition in a wide range of pH with a superior value of $D_h$ at 20 °C (Figure 5).

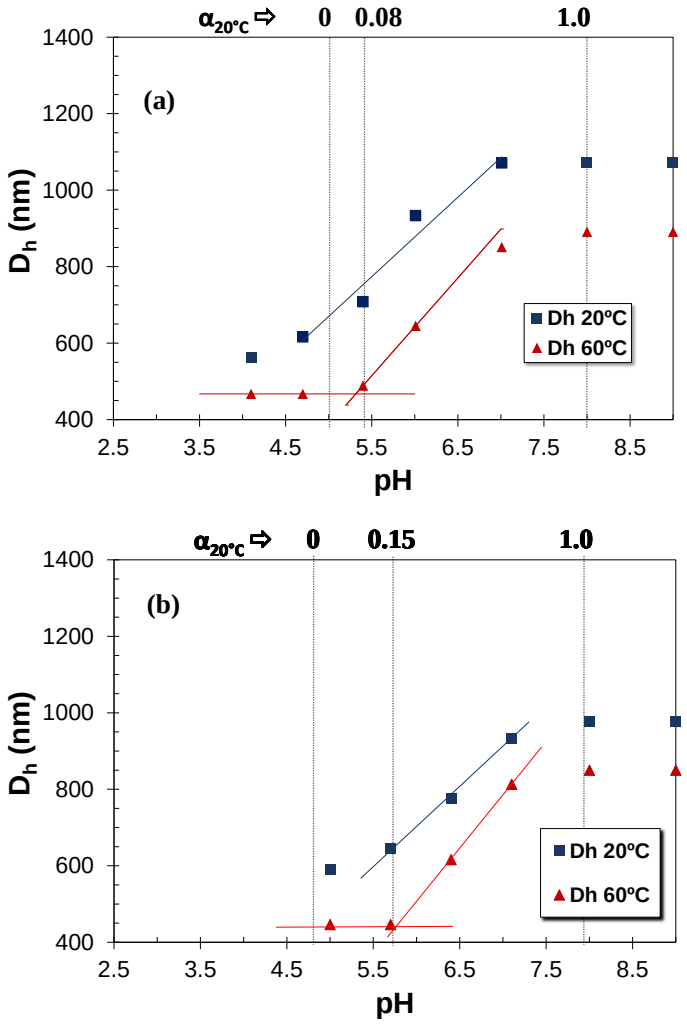

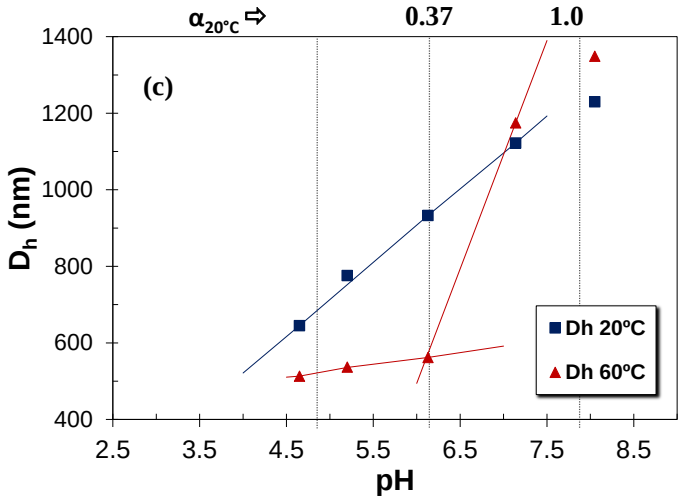


**Figure 5**. Hydrodynamic diameter $D_h$ (nm) versus pH at 20°C (red line) and 60°C (blue line) of P($MEO_2MA$-*co*-OEGMA-*co*-MAA) microgels crosslinked with (a) OEGDA, (b) MBA and (c) EGDMA.

The present study highlights a clear difference in the swelling behavior between the P($MEO_2MA$-*co*-OEGMA-*co*-MAA) microgels and P(NIPAM-*co*-MAA) microgels. While a sharp increase of the hydrodynamic diameter upon complete ionization of COOH units was observed for P($MEO_2MA$-*co*-OEGMA-*co*-MAA) microgels (Figure 5), a constant value of $D_h$ was recovered for P(NIPAM-*co*-MAA) microgels in the same range of pH (**Figure SI-5** in ESI). These results highlight the crucial role of the homogeneous distribution of COOH within the P($MEO_2MA$-*co*-OEGMA-*co*-MAA) microgels. On the basis of the Flory-Rehner theory, the swelling equilibrium of a gel is reached when the total osmotic pressure tends to zero.[63, 64] The osmotic pressure is the sum of mixing, elastic and ionic contributions. The ionization of carboxylic acid units tends to increase the internal osmotic pressure of the gel through electrostatic repulsions and counter-ions mobility, leading to additional swelling of the gel. [65] The low swelling ability of the P(NIPAM-*co*-MAA) microgels upon ionization of COOH units was ascribed to the closed-pack distribution of MAA units into PMAA-rich blocky sequences.[26] Thus, the elastic force of the rigid ionized PMAA-rich sequences couterbalances the ionic contribution, hence inhibiting the microgel swelling.

The profiles of $D_h$ versus pH depicted in Figure 5 suggest an influence of the network density on the pH-responsive behavior of the P($MEO_2MA$-*co*-OEGMA-*co*-MAA) microgels. At collapsed state (T = 60 °C), the sharp increase of $D_h$ versus pH is shifted from c.a. pH 5.4 (Figure 5a) for the homogeneously OEGDA crosslinked microgels to pH 6.1 (Figure 5c) for the EGDMA-crosslinked microgels exhibiting heterogeneities in the network with densely

crosslinked core and loosely crosslinked shell (Scheme 1 and Figure 2). As recently predicted theoretically,[66] such pH shift can be ascribed to the hindering of the ionization of the charged monomer by a higher local polymer concentration. The collapse of the loosely crosslinked chains together with the higher crosslinking density of the core can be at the origin of a higher local polymer concentration in EGDMA crosslinked microgels at 60°C in comparison with the homogeneously crosslinked OEGDA-based microgels .

The dual stimuli-responsive behavior of the P($MEO_2MA$-*co*-OEGMA-*co*-MAA) microgels can be rationalized by the calculation of the pH-induced swelling ratio ($\Phi_{pH} = (D_{h,\ pH\ 8})^3/(D_{h,\ pH\ 5})^3$) given at different temperatures and by the temperature-induced swelling ratio ($\Phi_{T°} = (D_{h,\ 20°C})^3/(D_{h,\ 60°C})^3$) provided at different pH values. The values of $\Phi_{pH}$ are gathered in Table 2 and compared with data obtained from literature for PNiPAM-based microgels with pseudo-homogeneous (P(NiPAM-*co*-AA)) or heterogeneous (P(NiPAM-*co*-MAA)) distribution of carboxylic acid units.

**Table 2. pH- and temperature induced swelling ratio ($\Phi$) of microgels.**

| Exp. | Structure | Crosslinker | $\Phi_{pH}$ | |
|---|---|---|---|---|
| | | | **20°C** | **60°C** |
| **1** | P($MEO_2MA$-*co*-OEGMA-*co*-MAA) | OEGDA | 7.9 | 6.9 |
| **2** | P($MEO_2MA$-*co*-OEGMA-*co*-MAA) | MBA | 6.2 | 6.9 |
| **3** | P($MEO_2MA$-*co*-OEGMA-*co*-MAA) | EGDMA | 16.8 | 18.2 |
| [a] | P(NIPAM-*co*-AA) | MBA | 3.5 | 1.5 |
| [a] | P(NIPAM-*co*-MAA) | MBA | 2.3 | 1.3 |

[a] From reference Hoare et al.[26] ($[MAA]_0$ corresponded to 6.1 mol-% of MAA units into the PNIPAM-based microgels and $\Phi_{pH}$ were calculated at 25°C and 70°C).

Among the different microgels, the EGDMA-crosslinked P($MEO_2MA$-*co*-OEGMA-*co*-MAA) microgels with dense core morphology and loosely crosslinked shell exhibit the highest pH-induced swelling ratio at both swollen and collapsed state (Exp. 3 in Table 2, $\Phi_{pH} \sim 17$). Previous studies performed with MBA-crosslinked PNIPAM microgels exhibiting dense core and loosely-crosslinked shell showed that the high swelling ability of such microgels was mainly driven by the flexible chains of the loosely crosslinked shell.[56] On the other hand, the

thin densely crosslinked shell of the MBA-crosslinked P($MEO_2MA$-*co*-OEGMA-*co*-MAA) microgels slightly reduces the pH-induced swelling ability at 20 °C ($\Phi_{pH,\ 20°C}$ = 6.2) in comparison with the homogeneously OEGDA crosslinked microgels ($\Phi_{pH,\ 20°C}$ = 7.9). The values of the pH-induced swelling ratio of the three types of the P($MEO_2MA$-*co*-OEGMA-*co*-MAA) microgels measured at both swollen (T = 20 °C) and collapsed state (T = 60 °C) are obviously higher by a factor of 2 to 13 than the ones reported in the literature for PNiPAM based microgels (see Table 2).[26]

The temperature-induced swelling ratio ($\Phi_{T°}$) of the P($MEO_2MA$-*co*-OEGMA-*co*-MAA) microgels was plotted as a function of pH as displayed in Figure 6. The variation of $\Phi_{T°}$ as a function of pH shows two distinguished intervals. Interval (I) corresponds to an increase of the temperature-induced swelling ratio ($\Phi_{T°}$), indicating the range of optimum degree of ionization of MAA ($0 < \alpha < 0.25$) to promote the most intense volume phase transition in response to temperature while keeping the colloidal stability. Interval (II) shows a decrease of $\Phi_{T°}$ by raising pH above pH 6 corresponding to a degree of ionization of MAA above 0.25. The progressive ionization of methacrylic acid into potassium carboxylate groups affords additional electrostatic repulsions which inhibit the shrinking of the network by increasing the microgel osmotic pressure.

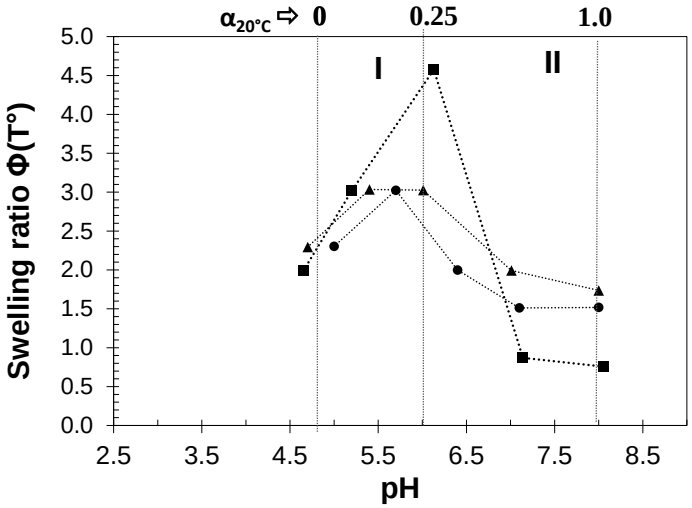


**Figure 6.** Temperature-induced swelling ratio ($\Phi_{T°}$) as a function of pH for P($MEO_2MA$-*co*-OEGMA-*co*-MAA) microgels crosslinked with OEGDA (▲), MBA (●) or EGDMA (■).

The EGDMA-crosslinked microgels exhibit a slightly different profile in comparison with the OEGDA or MBA-crosslinked microgels. Like for $\Phi_{pH}$, the highest value of the maximum $\Phi_{T°}$ was observed for the EGDMA-crosslinked microgels (Figure 6). It should be noticed that stable dispersions of OEGDA- and MBA-crosslinked microgels are systematically recovered over the

studied pH range (3 < pH < 9) while a macroscopic flocculation was observed at pH 3 for the EGDMA-crosslinked P($MEO_2$MA-*co*-OEGMA-*co*-MAA) microgels. The inter-particle potential is a balance between interactions arising from Van der Waals forces and long-range repulsive interactions caused by electrostatics. For a degree of ionization equal to zero (pH < 4.8), the decrease of pH value induces a progressive increase of salt concentration ($[HCl]_{pH3}$ = 0.2 mmol.$L^{-1}$). At pH 3, the interactions between the loosely crosslinked chains in EGDMA-crosslinked P($MEO_2$MA-*co*-OEGMA-*co*-MAA) microgels predominate while electrostatic repulsions of the initiator charges of the OEGDA- and MBA-crosslinked microgels are high enough to ensure stabilization of the hydrophobic microgels at pH 3 ($\alpha_{MAA} = 0$).

In summary of this part, we highlighted that the homogeneous distribution of the carboxylic acid groups within the P($MEO_2$MA-*co*-OEGMA-*co*-MAA) microgels is a critical parameter to promote a sharp collapse-to-swelling transition in response to both temperature and pH stimuli. The internal microgel structure, in terms of network homogeneity, drives the dual temperature and pH-responsive properties of the P($MEO_2$MA-*co*-OEGMA-*co*-MAA) microgels. Indeed, the loosely crosslinked chains in the shell of EGDMA-based microgels made of densely crosslinked core led to the highest values of pH- and temperature-induced swelling ratios but conferred instability in the presence of HCl salt. The OEGDA-crosslinked microgels formed by a homogeneous network remain stable in the presence of HCl salt and exhibit a temperature-induced swelling-to-collapse volume phase transition for pH values ranging from 3 to 9.

*Synthesis of thermoresponsive hybrid γ-$Fe_2O_3$ P($MEO_2$MA-co-OEGMA-co-MAA)) microgels: relationship between inner structure of microgels and loading of iron oxide nanoparticles.*

On the basis of our preliminary work,[67] we showed that The stable colloidal magnetic nanoparticles dispersed in water, also called ferrofluid ($D_h$ ~ 18 nm, see Figure SI-6 in ESI), were synthesized by the procedure previously described by Massart et al.[49, 50]. The recipe relies on the first synthesis of $Fe_3O_4$ magnetite nanoparticles by co-precipitation of iron salts in water, followed by the oxidation of $Fe_3O_4$ magnetite with nitric acid into γ-$Fe_2O_3$ maghemite. The stabilization of the dispersion of maghemite NPs in water is ensured by electrostatic repulsions of positively charged hydroxyl groups ($OH_2^+$) and non-flocculating nitrate counter-ions ($NO_3^-$) on nanoparticles surface. The preparation of the hybrid microgels is based on a straightforward two steps strategy. The first step consists in the incorporation of an aqueous dispersion of stable pre-formed iron oxide nanoparticles, which is driven by polar interactions between carboxylic acid units of microgels and the cationic magnetic NPs at pH 3. The second step relies on the

destabilization of the magnetic NPs inside the microgel by adjusting pH above the isoelectric point of the NP surface.[68] At pH 7.0, corresponding to the point of zero charge of the maghemite NPs, the neutral magnetic NPs are preferentially maintained inside the microgel network which are themselves stabilized by the potassium carboxylate functions and the persulfate groups (degree of ionization of COOH = 75-80 %, Figure 3).

The importance of the presence of MAA comonomer in the encapsulation of the NPs into the microgels was first investigated. For all systems used, the carboxylic acid-based comonomer distributed in the entire volume of the microgel plays a crucial role to promote interaction between microgels and magnetic NPs and to ensure the stability of the final hybrid microgels. Indeed, when using MAA-free microgels, NPs were expelled outside along with microgel flocculation (See Figure SI-7 in ESI). On the other hand, the strategy of NP encapsulation by polar interactions into the P($MEO_2MA$-*co*-OEGMA-*co*-MAA) microgels offers the unique opportunity to load high content of pre-formed magnetic NPs (up to 33 wt-% *vs.* microgel) in quantitative manner (see Table SI-1 and Figure SI-8 in ESI). It is interesting to note that the γ-$Fe_2O_3$-P($MEO_2MA$-*co*-OEGMA-*co*-MAA) hybrid microgels still exhibit a thermoresponsive swelling-to-collapse transition even for the highest content of magnetic NPs (33 wt-%). A constant value of VPTT of 35-40 °C was observed for 7.5 to 33 wt-% of NP content (see Figure 7 ).

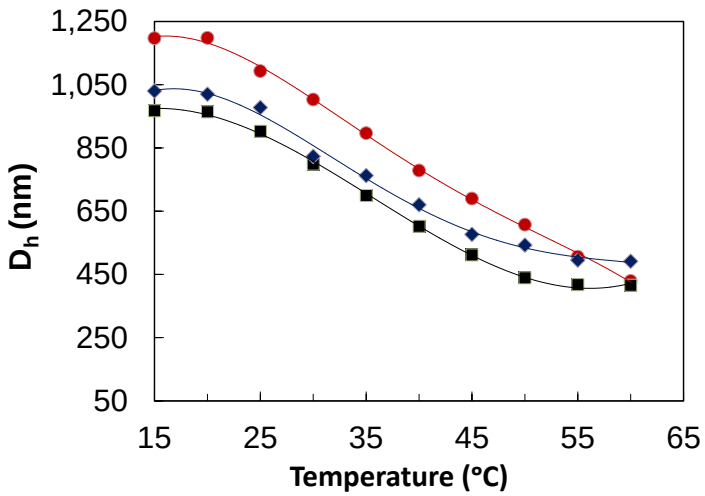


**Figure 7**. Hydrodynamic diameter (at pH 7) versus temperature of OEGDA-crosslinked P($MEO_2MA$-*co*-OEGMA-*co*-MAA) hybrid microgels loaded with differentweight fraction of γ-$Fe_2O_3$ : (●) 7 wt-%, (■) 16 wt-%, (◆) 33 wt-% vs. polymer.

The series of γ-$Fe_2O_3$/P($MEO_2MA$-*co*-OEGMA-*co*-MAA) microgels, crosslinked with different crosslinkers and initial weight fractions of magnetic NPs ($\Gamma_{Fe2O3,0}$), was characterized by transmission electron microscopy (TEM) in dry state (Figure 8). The spherical shape of the

initial P($MEO_2$MA-*co*-OEGMA-*co*-MAA) microgels ($\Gamma_{Fe2O3,0}$ = 0 wt-%) is maintained for the hybrid microgels. Unlike the example of itaconic acid-functionalized PNiPAM microgels showing extensive desorption of pre-formed magnetic NPs during the uptake step,[47] the present oligo(ethylene glycol)-based hybrid microgels do not exhibit any release of NP (Figure 8).

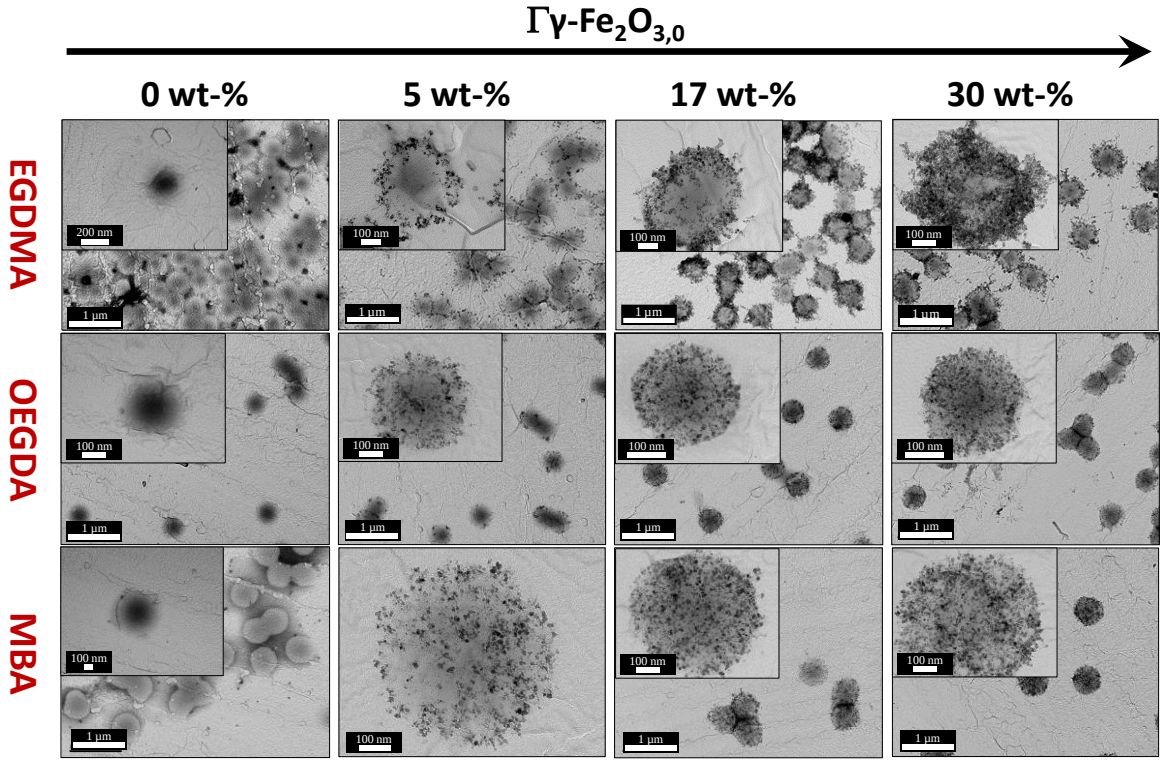


**Figure 8.** Transmission electron micrographs of P($MEO_2$MA-*co*-OEGMA-*co*-MAA) microgels and γ-$Fe_2O_3$-P($MEO_2$MA-*co*-OEGMA-*co*-MAA) hybrid microgels crosslinked with EGDMA, OEGDA or MBA. $\Gamma_{Fe2O3,0}$ is the initial weight content of NPs added into the microgel dispersion relative to the polymer weight.

TEM images of the hybrid γ-$Fe_2O_3$-P($MEO_2$MA-*co*-OEGMA-*co*-MAA) microgels crosslinked by OEGDA and MBA indicate that the average size of iron oxide nanoparticles is in the range of 10–20 nm and the increase of the nanoparticle loaded in the microgel does not lead to the increase of aggregation (**Figure 8**). While the inorganic nanoparticles are homogeneously distributed for OEGDA and MBA-crosslinked microgels, a preferential localization of the magnetic NPs at the periphery of the microgels is observed for the EGDMA-crosslinked P($MEO_2$MA-*co*-OEGMA-*co*-MAA) (**Figure 8**). It can be suggested that the densely crosslinked core of the EGDMA-crosslinked microgel limits the encapsulation of the NPs inside the core. Previous studies reported an increase of the VPTT or even its disappearance with

increasing the magnetic nanoparticle content for PNIPAM- or PVCL-based composite microgels exhibiting a heterogeneous distribution of magnetic nanoparticles.[21, 69] Pre-dominant inter-nanoparticle interactions were suggested to hamper the conformational transition of polymer segments.[21, 69] In the present case, the presence of a VPTT whatever the NP content in the OEGDA-crosslinked γ-$Fe_2O_3$-P($MEO_2MA$-*co*-OEGMA-*co*-MAA) hybrid microgels (Figure 7) is consistent with a rather homogeneous distribution of the nanoparticles in the volume of microgels. Finally, it should be noticed that in the case of MAA-free P($MEO_2MA$-*co*-OEGMA) microgels, the inorganic nanoparticles were obviously expelled outside the microgels (Figure SI-7 of in ESI). This supports the crucial role of the carboxylic acid functions for a successful loading of the preformed nanoparticles.

*Colloidal stability of microgels*

The stability of aqueous colloidal dispersion being an important criterion for their further use in cosmetic formulations for instance, the colloidal stability of the multi-responsive P($MEO_2MA$-*co*-OEGMA-*co*-MAA) microgels and of their hybrid homologues was investigated by turbidimetry analyses. The principles of measurements and additional experimental results are reported in more details in Supporting Information (see Figure SI-9). The relative light transmission ($\Delta T = T_t - T_0$) and of the relative light backscattering ($\Delta R = R_t - R_0$) were scanned along the entire height of the tube containing microgel dispersion at a solid content of 2.1 wt-% at different short-time intervals during several days.[70-73] This technique is relevant to give an insight into the clarification, flocculation and sedimentation rates (50 times earlier than the naked eye). [70-72] Figure 9 shows the evolution ΔT at the top of the tube, characteristic of the clear layer formed by the clarification process. First, a long term stability of the OEGDA-crosslinked P($MEO_2MA$-*co*-OEGMA-*co*-MAA) microgels was observed as none loss of transmission was observed for 100 hours and the plateau of ΔT reached only after 300 h (Figure 9). Moreover, a constant value of backscattering intensity close to zero was observed in the middle zone and the formation of the sedimentation layer was accordingly very long (Figure SI-10 and Figure SI-11 in ESI). Such trend is the sign of a sedimentation phenomenon occurring by migration of individual particles in the absence of flocculation occurring by aggregation.[73]

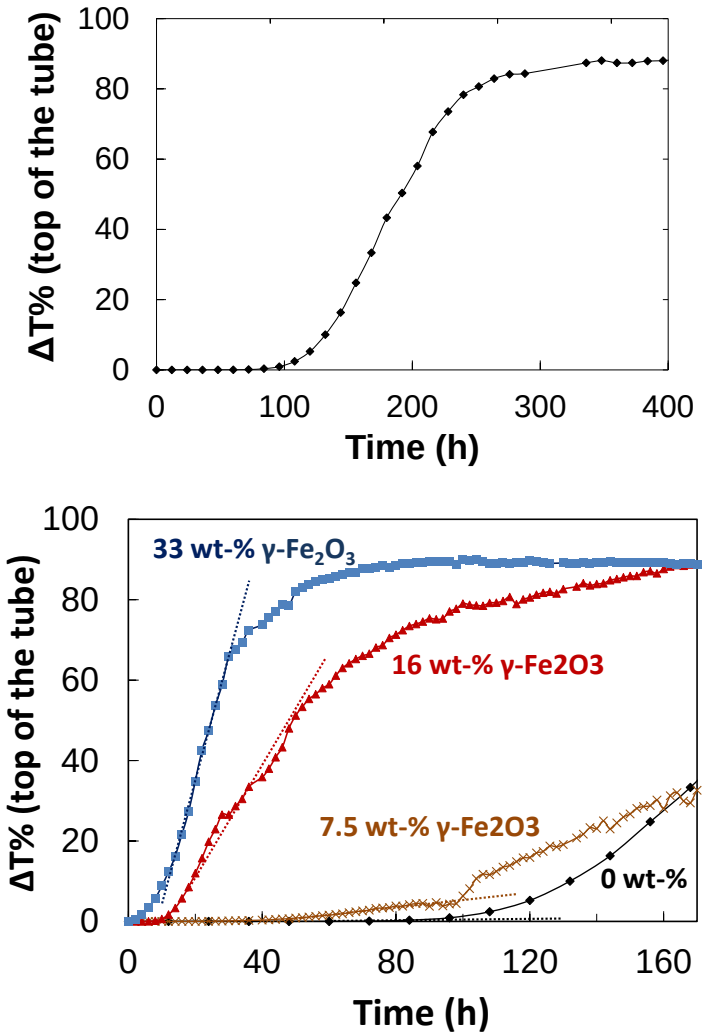


**Figure 9**. Relative transmission intensity ΔT (in %) at the top of the tube (H= 35.6 mm ± 1.0) as a function of time for OEGDA-crosslinked P($MEO_2MA$-*co*-OEGMA-*co*-MAA) microgels (top, 0 wt-% of NP, ◆) and for γ-$Fe_2O_3$-P($MEO_2MA$-*co*-OEGMA-*co*-MAA) hybrid microgels (bottom, 0 (◆), 7.5 (×), 16 (▲), 33 (■) wt-% of NP) as a function of time (solid content $\tau$ = 2.1 wt-%).

The content of magnetic iron oxide nanoparticles predominantly impacts the colloidal stability of the hybrid microgels as displayed in Figure 9. The clarification rate of the microgels loaded with 7.5 wt-% of NPs is close to the one of the initial microgels free of NPs while a sharp increase of the clarification rate is observed for NP content of 16 to 33 wt-% (Figure 9). The higher values of the sedimentation rate in comparison with the clarification rate (factor of 10 to 100, see Table SI-2 in ESI) and the decrease of the relative backscattering intensity in the middle of the tube both reveal that the migration of the hybrid microgels is governed by concomitant sedimentation/flocculation phenomena. According to the Stokes' law of sedimentation, the

migration rate ($v$) of dispersed colloids should increase with the difference of density between the colloids and the continuous phase (see equation 9 with $g$ the gravitational acceleration (m.s$^{-2}$), $\rho_{\text{hybrid microgel}}$ and $\rho_{\text{water}}$ respectively the mass density (in kg.m$^{-3}$) of the hybrid microgel and water, $D_h$ the hydrodynamic diameter of the hybrid microgel measured at 30°C (m) and $\eta$ the dynamic viscosity of the dispersed medium (kg.m$^{-1}$.s$^{-1}$)).

$$v = \frac{D_h^2 \, g(\rho_{swollen\ hybrid\ microgel} - \rho_{water,30\,℃})}{18\eta} \quad (9)$$

Herein, the migration rate was calculated from the clarification height *vs* time (Figure SI-13 in ESI) and the mass density of the hybrid microgels was calculated on the basis of the weight fraction of inorganic nanoparticles (see Table SI-3 in ESI). A linear evolution of the migration rate of the present γ-$Fe_2O_3$-P($MEO_2MA$-*co*-OEGMA-*co*-MAA) hybrid microgels with the density of hybrid microgels confirms the Stokes' law of sedimentation (Figure 10).

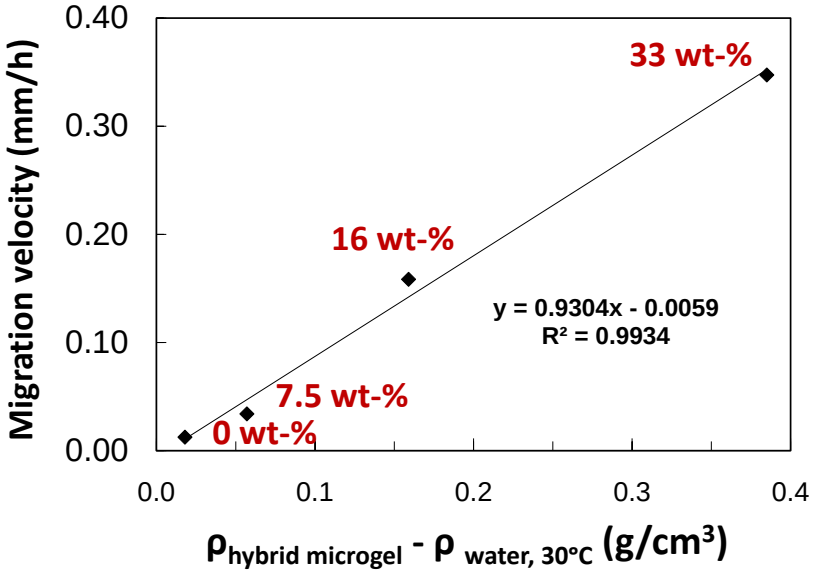


**Figure 10.** Migration velocity as a function of [$\rho_{\text{hybrid microgel}} - \rho_{\text{water}}$] of hybrid γ-$Fe_2O_3$-P($MEO_2MA$-*co*-OEGMA-*co*-MAA) microgels with NP content ranging from 0 to 33 wt-%.

It is worth to note that the present γ-$Fe_2O_3$-P($MEO_2MA$-*co*-OEGMA-*co*-MAA) hybrid microgels still exhibit interesting colloidal features in comparison with the hybrid PNIPAM-based microgels. Indeed, previous works on PNIPAM-based microgel encapsulated with titanium oxide ($TiO_2$) for instance demonstrated the fast sedimentation of the hybrid microgel in less than 5 min with 25 wt-% of NP loading.[74] Other studies pointed out the immediate loss of colloidal stability following the encapsulation of various inorganic nanoparticles in PNIPAM-based,[69, 75] and PVCL-based[76, 77] microgels. They ascribed such loss of colloidal

stability to an increase of density related to the encapsulation of the inorganic NPs. In the present work, the increase of the γ-$Fe_2O_3$ content in P($MEO_2$MA-*co*-OEGMA-*co*-MAA) microgel increases the sedimentation and clarification rates but stability is still maintained for more than 50 hours.

## CONCLUSIONS

In conclusion, the present work reported the synthesis of poly(di(ethylene glycol) methyl ether methacrylate-*co*-oligo(ethylene glycol) methyl ether methacrylate-*co*-methacrylic acid) (P($MEO_2$MA-*co*-OEGMA-*co*-MAA)) microgels by one-pot precipitation polymerization carried out in aqueous dispersed media. The relationship between the inner structure of the different microgels on their multi-responsive behavior was investigated. The pH- or temperature-induced swelling ratio of the P($MEO_2$MA-*co*-OEGMA-*co*-MAA) microgels can be tuned by the crosslinking density, which depends on the chemical nature of the crosslinker (EGDMA, OEGDA or MBA). The highest pH-induced swelling ratio ($\Phi_{pH} \sim 17$) was observed for the EGDMA-crosslinked microgels exhibiting densely crosslinked core and loosely crosslinked shell. Such high swelling ratio is ascribed to the higher conformation change ability of the very loosely crosslinked high molar mass polymer chains of the microgel shell. Both the monitoring of the individual co-monomer conversion and the absence of polyelectrolyte effect on the ionization of PMAA units converge to show the homogeneous distribution of the MAA units within the microgels whatever the nature of the crosslinker. It should be noticed that such microstructure offers the opportunity to maintain the pH-induced swelling behavior of microgels at both swollen and collapsed state (T =20 °C and 60°C) with a sharp increase of their hydrodynamic diameter by increasing pH. The volume phase transition temperature of the P($MEO_2$MA-*co*-OEGMA-*co*-MAA) microgels shifted from 34 °C for protonated carboxylic acid functions to 55 °C for a complete ionization of MAA units. An unprecedented narrow swelling-to-collapse transition was observed in the entire pH range (from pH 3 to pH 9) for OEGDA-crosslinked P($MEO_2$MA-*co*-OEGMA-*co*-MAA) microgels while broadening of the temperature-induced transition was systematically observed with ionization of PNiPAM-based microgels. The evolution of light transmission and backscattering with time highlighted a long term stability for the P($MEO_2$MA-*co*-OEGMA-*co*-MAA) microgels free of nanoparticles. These oligo(ethylene glycol) based microgels proved to be ideal candidates to synthesize hybrid magnetic microgels by a straightforward method based on the polar interaction-driven loading of pre-formed iron oxide maghemite nanoparticles (NP) in the absence of any NP release.

Interestingly, the hybrid microgels loaded with up to 33 wt-% of nanoparticles retain a volume phase transition temperature at 35-40 °C, which supports a homogeneous distribution of the magnetic nanoparticles inside the volume of the microgel. A unique stability of the hybrid microgels was observed over more than 50 hours with a linear variation of the migration rate versus the density of the hybrid microgels according to the Stokes' law. The microgel stability associated with their dual stimuli-responsive behavior of the biocompatible oligo(ethylene glycol)-based microgels open interesting perspectives for different fields of applications such as smart delivery systems of active molecules.

**Acknowledgements**

The authors are grateful to LVMH for funding MB PhD, CNRS and UPPA for MS and LB. The authors would like to acknowledge T. Pouget (LVMH), L. Neau (LVMH) and A. Khoukh (IPREM-EPCP) for their support for respectively Turbiscan, TEM and NMR analyses. We also thank J. Rieger and L. Bouteiller (UMR8232) for supplying Nanosizer90 for DLS of hybrid microgels. The authors are grateful to Dr. O. Borisov (IPREM-EPCP) and E. Gombart (LVMH) for fruitful discussions.

**References**

1. R. H. Pelton and P. Chibante, *Colloids and Surfaces*, 1986, **20**, 247-256.
2. I. Berndt, J. S. Pedersen and W. Richtering, *J. Am. Chem. Soc.*, 2005, **127**, 9372-9373.
3. Z. S. An, Q. H. Shi, W. Tang, C. K. Tsung, C. J. Hawker and G. D. Stucky, *J. Am. Chem. Soc.*, 2007, **129**, 14493-14499.
4. X. Hu, Z. Tong and L. A. Lyon, *J. Am. Chem. Soc.*, 2010, **132**, 11470-11472.
5. Y. Hertle and T. Hellweg, *J. Mater. Chem. B*, 2013, **1**, 5874-5885.
6. S. Sun and P. Wu, *Macromolecules*, 2013, **46**, 236-246.
7. S. Sun and P. Wu, *J. Phys. Chem. B*, 2011, **115**, 11609-11618.
8. K. Kubota, S. Fujishige and I. Ando, *J. Phys. Chem.*, 1990, **94**, 5154-5158.
9. M. Karg, I. Pastoriza-Santos, B. Rodriguez-González, R. von Klitzing, S. Wellert and T. Hellweg, *Langmuir*, 2008, **24**, 6300-6306.
10. Y. Wang, J. Nie, B. Chang, Y. Sun and W. Yang, *Biomacromolecules*, 2013, **14**, 3034-3046.
11. G. M. Eichenbaum, P. F. Kiser, A. V. Dobrynin, S. A. Simon and D. Needham, *Macromolecules*, 1999, **32**, 4867-4878.
12. M. J. Serpe, K. A. Yarmey, C. M. Nolan and L. A. Lyon, *Biomacromolecules*, 2005, **6**, 408-413.
13. N. M. B. Smeets and T. Hoare, *J. Polym. Sci. A Polym. Chem.*, 2013, **51**, 3027-3043.
14. S. Lou, S. Gao, W. Wang, M. Zhang, J. Zhang, C. Wang, C. Li, D. Kong and Q. Zhao, *Nanoscale*, 2015, **7**, 3137-3146.
15. C. Fenzl, T. Hirsch and O. S. Wolfbeis, *Angew. Chem. Int. Ed.*, 2014, **53**, 3318-3335.
16. M. R. Islam and M. J. Serpe, *Macromolecules*, 2013, **46**, 1599-1606.

17. M. Destribats, M. Eyharts, V. Lapeyre, E. Sellier, I. Varga, V. Ravaine and V. Schmitt, *Langmuir*, 2014, **30**, 1768-1777.
18. A. J. Morse, S. P. Armes, K. L. Thompson, D. Dupin, L. A. Fielding, P. Mills and R. Swart, *Langmuir*, 2013, **29**, 5466-5475.
19. M. Karg and T. Hellweg, *J. Mater. Chem.*, 2009, **19**, 8714-8727.
20. B. H. Juarez and L. M. Liz-Marzan, *Z. Phys. Chem.*, 2015, **229**, 263-282.
21. A. Pich, S. Bhattacharya, Y. Lu, V. Boyko and H.-J. P. Adler, *Langmuir*, 2004, **20**, 10706-10711.
22. D. Jancezewski, N. Tomczak, M.-Y. Han and G. J. Vancso, *Macromolecules*, 2009, **42**, 1801-1804.
23. E. Pavlopoulou, G. Portale, K. E. Christodoulakis, M. Vamvakaki, W. Bras and S. H. Anastasiadis, *Macromolecules*, 2010, **43**, 9828-9836.
24. Z. Dai and T. Ngai, *J. Polym. Sci. A Polym. Chem.*, 2013, **51**, 2995-3003.
25. T. Hoare and R. Pelton, *Macromolecules*, 2004, **37**, 2544-2550.
26. T. Hoare and R. Pelton, *Langmuir*, 2006, **22**, 7342-7350.
27. M.-h. Kwok, Z. Li and T. Ngai, *Langmuir*, 2013, **29**, 9581-9591.
28. I. Varga, T. Gilányi, R. Mészáros, G. Filipcsei and M. Zrínyi, *J. Phys. Chem. B*, 2001, **105**, 9071-9076.
29. R. Acciaro, T. Gilányi and I. Varga, *Langmuir*, 2011, **27**, 7917-7925.
30. S. Meyer and W. Richtering, *Macromolecules*, 2005, **38**, 1517-1519.
31. H. Vihola, A. Laukkanen, L. Valtola, H. Tenhu and J. Hirvonen, *Biomaterials*, 2005, **26**, 3055-3064.
32. A. Imaz and J. Forcada, *J. Polym. Sci. A Polym. Chem.*, 2010, **48**, 1173-1181.
33. H. Vihola, A. Laukkanen, L. Valtola, H. Tenhu and J. Hirvonen, *Biomaterials*, 2005, **26**, 3055-3064.
34. A. Imaz and J. Forcada, *J. Polym. Sci. A Polym. Chem.*, 2011, **49**, 3218-3227.
35. J. F. Lutz, S. Stiller, A. Hoth, L. Kaufner, U. Pison and R. Cartier, *Biomacromolecules*, 2006, **7**, 3132-3138.
36. S. V. Lale, R. G. Aswathy, A. Aravind, D. S. Kumar and V. Koul, *Biomacromolecules*, 2014, **15**, 1737-1752.
37. L. Yu, Z. Shi, L. Gao and C. Li, *Journal of biomedical materials research. Part A*, 2015, **103**, 2987-2997.
38. M. Ulasan, E. Yavuz, E. U. Bagriacik, Y. Cengeloglu and M. S. Yavuz, *Journal of Biomedical Materials Research Part A*, 2015, **103**, 243-251.
39. J.-F. Lutz, Ö. Akdemir and A. Hoth, *J. Am. Chem. Soc.*, 2006, **128**, 13046-13047.
40. J.-F. F. Lutz, *Adv. Mater.*, 2011, **23**, 2237-2243.
41. J.-F. F. Lutz and A. Hoth, *Macromolecules*, 2006, **39**, 893-896.
42. C. Chi, T. Cai and Z. Hu, *Langmuir*, 2009, **25**, 3814-3819.
43. T. Cai, M. Marquez and Z. Hu, *Langmuir*, 2007, **23**, 8663-8666.
44. T. Zhou, W. Wu and S. Zhou, *Polymer*, 2010, **51**, 3926-3933.
45. Y. Chen, N. Ballard and S. A. F. Bon, *Polym. Chem.*, 2013, **4**, 387-392.
46. S. Wellert, D. Kesal, S. Schoen, R. von Klitzing and K. Gawlitza, *Langmuir*, 2015, **31**, 2202-2210.
47. F. Sauzedde, A. Elaissari and C. Pichot, *Colloid & Polymer Science*, 1999, **277**, 1041-1050.
48. J. Zhang, S. Xu and E. Kumacheva, *J. Am. Chem. Soc.*, 2004, **126**, 7908-7914.
49. R. Massart, *IEEE Trans. Magn.*, 1981, **17**, 1247-1248.
50. A. Bee, R. Massart and S. Neveu, *J. Magn. Magn. Mater.*, 1995, **149**, 6-9.
51. S. Kawaguchi, A. Yekta and M. A. M. Winnik, *J. Colloid Interface Sci.*, 1995, **176**, 362-369.

52. T. Gilanyi, I. Varga, R. Meszaros, G. Filipcsei and M. Zrinyi, *PCCP*, 2000, **2**, 1973-1977.
53. in *The MAK-Collection for Occupational Health and Safety*, Wiley-VCH Verlag GmbH & Co. KGaA, 2002, pp. 248-270.
54. P. Hazot, T. Delair, C. Pichot, J.-P. Chapel and A. Elaissari, *Comptes Rendus Chimie*, 2003, **6**, 1417-1424.
55. A. Guillermo, J. P. C. Addad, J. P. Bazile, D. Duracher, A. Elaissari and C. Pichot, *J. Polym. Sci., Part B: Polym. Phys.*, 2000, **38**, 889-898.
56. B. R. Saunders, *Langmuir*, 2004, **20**, 3925-3932.
57. M. Stieger, W. Richtering, J. S. Pedersen and P. Lindner, *J. Chem. Phys.*, 2004, **120**.
58. X. Wu, R. H. Pelton, a. E. Hamielec, D. R. Woods and W. McPhee, *Colloid & Polymer Science*, 1994, **272**, 467-477.
59. I. Borukhov, D. Andelman, R. Borrega, M. Cloitre, L. Leibler and H. Orland, *J. Phys. Chem. B*, 2000, **104**, 11027-11034.
60. O. Colombani, E. Lejeune, C. Charbonneau, C. Chassenieux and T. Nicolai, *J. Phys. Chem. B*, 2012, **116**, 7560-7565.
61. P. Sheikholeslami, C. Ewaschuk, S. Ahmed, B. Greenlay and T. Hoare, *Colloid & Polymer Science*, 2012, **290**, 1181-1192.
62. S. Zhou and B. Chu, *J. Phys. Chem. B*, 1998, **102**, 1364-1371.
63. P. J. Flory and J. Rehner, *J. Chem. Phys.*, 1943, **11**, 512-520.
64. P. J. Flory and J. Rehner, *J. Chem. Phys.*, 1943, **11**, 521-526.
65. T. Hoare and R. Pelton, *The journal of physical chemistry. B*, 2007, **111**, 11895-11906.
66. A. A. Polotsky, F. A. Plamper and O. V. Borisov, *Macromolecules*, 2013, **46**, 8702-8709.
67. M. Boularas, E. Gombart, J.-F. Tranchant, L. Billon and M. Save, *Macromol. Rapid Commun.*, 2015, **36**, 79-83.
68. I. T. Lucas, S. Durand-Vidal, E. Dubois, J. Chevalet and P. Turq, *J. Phys. Chem. C*, 2007, **111**, 18568-18576.
69. J. Rubio-Retama, N. E. Zafeiropoulos, C. Serafinelli, R. Rojas-Reyna, B. Voit, E. Lopez Cabarcos, M. Stamm and E. L. Cabarcos, *Langmuir*, 2007, **23**, 10280-10285.
70. N. Azema, *Powder Technol.*, 2006, **165**, 133-139.
71. C. Lemarchand, *Int. J. Pharm.*, 2003, **254**, 77-82.
72. R. Vie, N. Azema, J. C. Quantin, E. Touraud and M. Fouletier, *Colloids and Surfaces A: Physicochem. Eng. Aspects*, 2007, **298**, 192-200.
73. O. Mengual, G. Meunier, I. Cayre, K. Puech and P. Snabre, *Colloids and Surfaces A: Physicochem. Eng. Aspects*, 1999, **152**, 111-123.
74. C. A. Coutinho and V. K. Gupta, *J. Colloid Interface Sci.*, 2007, **315**, 116-122.
75. M. Laurenti, P. Guardia, C.-C. Rafael, P.-J. Jorge, F.-B. Antonio, L.-C. Enrique and R.-R. Jorge, *Langmuir*, 2011, **27**, 10484-10491.
76. S. Bhattacharya, F. Eckert, V. Boyko and A. Pich, *Small*, 2007, **3**, 650-657.
77. A. Pich, J. Hain, Y. Lu, V. Boyko, Y. Prots and H.-J. Adler, *Macromolecules*, 2005, **38**, 6610-6619.